Friction **4**(4): 347–358 (2016)
DOI 10.1007/s40544-016-0131-9
ISSN 2223-7690
CN 10-1237/TH

RESEARCH ARTICLE

Identifying the optimal interfacial parameter correlated with hydrodynamic lubrication

Liang GUO[1,*], Patrick WONG[1], Feng GUO[2]

[1] *Department of Mechanical and Biomedical Engineering, City University of Hong Kong, Hong Kong, China*

[2] *Mechanical Engineering Department, Qingdao Technological University, Qingdao 266033, China*

Received: 26 May 2016 / Revised: 22 September 2016 / Accepted: 13 November 2016

Abstract: The effects of boundary (liquid/solid) slip on hydrodynamics are well recognized. However, it is extremely difficult to quantify *in-situ* boundary slip in a lubrication contact. Therefore, an effective interfacial parameter that is well correlated with the lubrication effect is of practical significance. This paper presents an examination of common interfacial parameters, including surface tension, contact angle, contact angle hysteresis, and a recently proposed spreading parameter. Specimen surfaces of different hydro/oleophobicity were prepared and characterized using the aforementioned interfacial parameters. These samples were further used as bearing surfaces in hydrodynamic lubrication tests. The correlations of these parameters with the measured lubricating film thickness were examined and compared. The key parameter closely related to the hydrodynamic effect was identified.

Keywords: bearing; slip; oleophobicity; thin hydrodynamic film

1 Introduction

The no-slip boundary condition adopted by the classical hydrodynamic lubrication theory is based on the idea that the adhesive force between solid and liquid molecules at the solid/liquid boundary is stronger than the cohesive force among liquid molecules. However, it may not apply to physical situations. For example, surfaces may be contaminated by other adsorbed environmental molecules, or by oxidation, thereby reducing the surface energy. Furthermore, the advent of super-hydrophobic surfaces has enabled a liquid to slip on the outer molecular layer of a solid surface. Qualitative and quantitative studies on the relative motion at the solid/liquid interface have long been a focus of surface science research. Recently, relevant phenomena have also attracted considerable attention in the engineering tribology community, based on the idea of friction reduction through boundary slip [1–4]. The onset and magnitude of slip at the solid/liquid boundary in a lubricating system are determined by the competition between the magnitude of the viscous strength of the lubricant and the adhesive force between the liquid and solid molecules. Boundary slip occurs only when the shear stress at the solid/liquid interface is sufficiently large to overcome the adhesive strength between the solid and liquid molecules [5–7].

To quantify the strength of the solid/liquid interface, different interfacial parameters have been proposed. The most popular is contact angle. Conceptually, a large contact angle implies a small interfacial force and a non-wetting solid/liquid contact. This concept was supported by Hild et al. [8], who reported a significant drop in hydrodynamic force on a non-wetting surface and detected that viscous forces are significantly less in hydrophobic surfaces when compared to hydrophilic surfaces. Baudry et al. [9] studied the drainage force between a sphere and a plane coated with two different coatings using the surface force apparatus technique. The researchers spotted

* Corresponding author: Liang GUO.
E-mail: liangguo3-c@my.cityu.edu.hk

the boundary slip occurs only with the plane coated with thiol coating (with a relatively large advancing contact angle (θ_A: 94°), but not with cobalt coating (θ_A: 62°). Tretheway and Meinhart [10] also arrived at the same conclusion in their studies using particle image velocimetry. Zhu and Granick [6] found that the amount of slip increased with the contact angle when the shear rate in their squeeze film tests exceeded a critical value. Guo et al. [11] recently studied the effect of wettability on lubricant film thickness with optical interferometry, and their results showed that a large contact angle corresponded to a thin film thickness. Nevertheless, different conclusions were drawn by other investigators on the relationship between contact angle/wettability and friction of a lubricated contact. Bongaerts et al. [12] determined that there was no relationship between wettability and hydrodynamic force in the elasto-hydrodynamic lubrication regime. Joseph and Tabeling [13] found no difference in the magnitude of slip on a hydrophobic or a hydrophilic surface when measuring the velocity profile of water flow on various surfaces.

Considering the contradictory conclusions of the aforementioned studies, contact angle is not an effective parameter for describing the intermolecular strength of solids and liquids. Identifying a key interfacial parameter that best correlates with hydrodynamic lubrication is beneficial to the design of a hydrodynamic lubricated system. Boundary slip may be quantified in a lab environment through direct observation [10, 13, 14], but *in-situ* measurement of boundary slip is extremely difficult, although a recent attempt by Ponjavic et al. [15] showed that it is not impossible. Thus, this paper presents an examination of common interfacial parameters, including surface tension, contact angle, contact angle hysteresis (CAH), and a recently proposed spreading parameter (SP) [16, 17]. Hydrodynamic lubrication tests were conducted using the model surfaces of different interfacial parameters. Correlations of the film-forming capability of different bearing surfaces with their various interfacial parameters were conducted and compared.

2 Interfacial parameters

The common interfacial parameters can be classified as either static or dynamic, depending on the methods of their measurements. The former includes contact angle and surface energy, whereas the latter includes CAH. The typical interfacial parameters are described briefly in the following sections.

2.1 Contact angle

Contact angle is defined as the elevated angle of the tangent at the boundary of the profile of a tiny liquid droplet and the solid plane, as illustrated in Fig. 1. The interface in which the three phases (liquid, solid, and vapor) meet is referred to as the "three-phase contact line". If the contact angle formed by a small drop of water and a solid surface is less than 90°, the solid surface is generally considered hydrophilic, and the wetting of the solid surface is favorable, thereby indicating that water tends to spread on the surface. In contrast, a solid surface is hydrophobic and water has difficulty spreading on the surface if the contact angle is greater than 90°. A contact angle is the resultant of the equilibrium of three surface tensions, which can be expressed by Young's equation [18],

$$\cos\theta = \frac{\gamma_S - (\gamma_{SL} + \pi_e)}{\gamma_L} \tag{1}$$

where γ_{SL} , γ_S and γ_L are, respectively, the solid/liquid, the solid/vapor and the liquid/vapor interfacial tensions, π_e is the change in surface free energy of the solid surface resulting from the adsorption of another substance, and θ is the Young's contact angle (the contact angle formed by a liquid drop and an ideal solid surface). The volume of the droplet must be very small (less than 10 μL), i.e., the weight of the water droplet can be ignored. Furthermore, the measurements are typically taken in a controlled environment under atmospheric pressure, and π_e can also be neglected. Hence, contact angle is generally expressed as

$$\theta = \cos^{-1}\left(\frac{\gamma_S - \gamma_{SL}}{\gamma_L}\right) \tag{2}$$

It is commonly accepted that the contact angle of a liquid on a solid surface can be related to intermolecular attractive force. A "sticky" surface results in a small contact angle because of the strong affinity or adhesion between the liquid and the surface. However, this

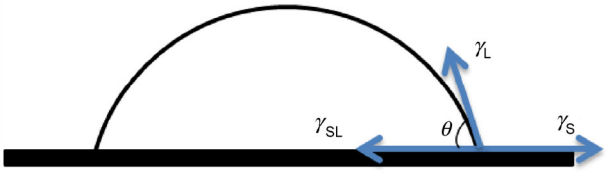

Fig. 1 Illustration of contact angle formed by a sessile drop on a homogenous smooth surface.

phenomenon is not always valid. For example, Wang et al. [19] developed a technique for fabricating superoleophobic surfaces with a switchable adhesion force with oil drops. With increasing UV treatment time, the sliding angle of the oil drop changes from approximately 0° to 90°, whereas the contact angle is only reduced by approximately 10%, as shown in Fig. 2(a). Examples of surfaces with large contact angles and strong adhesive forces can be found in nature such as a rose petal surface [20]. As shown in Fig. 2(b), the contact angle formed between water and Rosa, *cv*. Bairage (a type of rose petal) is large, whereas the water drop remains suspended on the petal surface even if the tilting angle is turned by 180°. Therefore, representing the adhesive force between liquid and solid molecules solely via contact angle is inaccurate.

2.2 Kalin's spreading parameter, SP

Kalin and Polajnar [16, 17] derived a SP to describe the wetting phenomenon based on the difference in the work of adhesion and cohesion.

$$\mathrm{SP} = W_a - W_c = \gamma_S - (\gamma_{SL} + \gamma_L) \tag{3}$$

SP is the resultant of the competitiveness between the adhesive and cohesive work, which is similar to the concept of contact angle. However, Kalin and Polajnar [16, 17] proved that instead of contact angle, this parameter can effectively describe the actual wetting property of diamond-like-carbon coated surfaces and steel surfaces with oils (PAOs were used in their study). The SP was derived using Young's equation (Eq. (2)) and the Owens–Wendt–Rabel–Kaelble (OWRK) model [21]. The OWRK model considers both the dispersive and polar components of the solid and liquid surface tensions and can be expressed as

$$\mathrm{SP} = 2\left(\sqrt{\gamma_S^D}\sqrt{\gamma_L^D} + \sqrt{\gamma_S^P}\sqrt{\gamma_L^P} - \gamma_L\right) \tag{4}$$

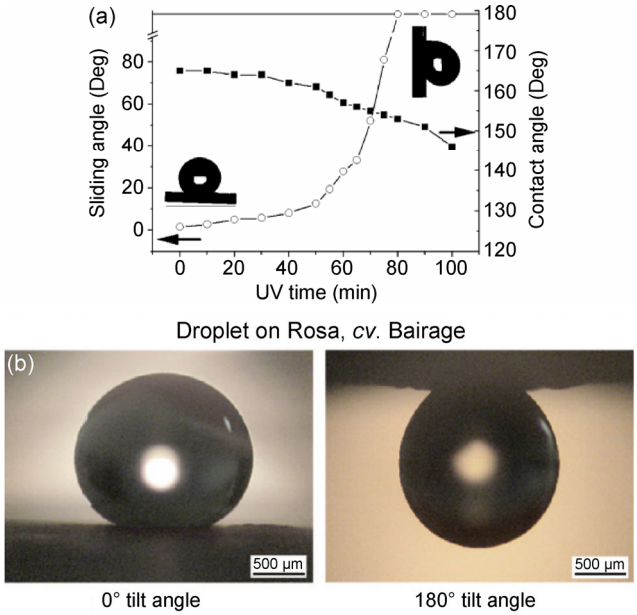

Fig. 2 Example of strong affinity between a liquid drop with an exceedingly large contact angle and a surface (excerpt from Refs. [19] and [20]).

where γ_S^D and γ_S^P represent the dispersive and polar components of the solid surface tension, respectively, and γ_L^D and γ_L^P denote the dispersive and polar components of the liquid surface tension, respectively. A noteworthy phenomenon was recorded by Kalin and Polajnar [16, 17] that for surfaces of high SP, the magnitude of the contact angle reduced significantly in the first few seconds after the oil was dropped on the surface, and before it became steady. In contrast, one sample surface had a much higher contact angle than all other sample surfaces, as well as the lowest SP (it was a negative number, whereas all others were positive). The contact angle of this sample surface did not vary with time, and the sessile drop obtained its final form once it rested on the solid surface. The results showed that SP can reflect the spreading ability of a liquid on a solid plane.

2.3 Advancing contact angle and receding contact angle

Lubrication processes are dynamic in nature, whereas the contact angle is a static measurement. The contact angle of a solid plane falls into a range of values in which the sessile drop achieves a shape with its free surface energy at the minimum, and the equilibrium contact angle is obtained. If the volume of the droplet

is increased steadily, then the contact angle increases, but without an increase in the solid/liquid contact area. The maximum contact angle that can be achieved before the expansion of the contact area is defined as the advancing contact angle, θ_A. With the steady removal of liquid from the droplet, the contact angle decreases until the contact area contracts. The minimum contact angle is termed as the receding contact angle, θ_R. Parameters θ_A and θ_R are both obtained under particular conditions and can therefore be considered dynamic.

2.4 $\cos\theta_R - \cos\theta_A$

While measuring the advancing and receding contact angles, the sample liquid pumps in and out of the droplet until the impending motion of the three-phase contact line occurs. The contact angles, θ_A and θ_R, can be expressed in the form of a modified Young's equation as in the following

$$\cos\theta_A = \frac{\gamma_S - (\gamma_{SL} + F_{in})}{\gamma_L} \tag{5}$$

$$\cos\theta_R = \frac{\gamma_S - (\gamma_{SL} - F_{out})}{\gamma_L} \tag{6}$$

where F_{in} and F_{out} are extra forces per unit length on the liquid/solid contact line because of the liquid flowing into and out of the droplet. Thus,

$$\cos\theta_R - \cos\theta_A = \frac{F_{in} + F_{out}}{\gamma_L} \tag{7}$$

2.5 Contact angle hysteresis (CAH)

CAH is defined as the difference of the advancing and receding contact angles:

$$\text{CAH} = \theta_A - \theta_R \tag{8}$$

Yaminsky [22] discussed the importance of solid/liquid molecular adsorption to wettability and correlated CAH with the static friction effect. When the motion of the three-phase contact line of the drop (during the addition or removal of liquid) is hindered by the intermolecular forces or surface roughness, the magnitude of contact angle can vary in a range. Extrand [23] indicated that CAH is not caused by roughness, but by molecular interactions at the contact line. Yaminsky [22] and Extrand [23] noted that CAH can reflect the solid/liquid adhesive force or the affinity between liquid and solid, particularly if the solid surface is perfectly flat and homogeneous. This idea was later theoretically proven by Whyman et al. [24] who derived the following expression based on a thermodynamic principle:

$$\text{CAH} = \left(\frac{8U}{\gamma_L R}\right)^{1/2} \frac{(1-\cos\theta)^{1/12}(2+\cos\theta)^{2/3}}{2^{1/3}(1+\cos\theta)^{1/4}} \tag{9}$$

where R is the radius of the liquid drop before deposition on solid surface, and U is the potential energy barrier. The criterion for liquid molecules sliding on an array of solid molecules is to overcome the potential energy barrier. A high energy barrier corresponds to a large adhesive force. Equation (9) shows that the potential energy barrier is related to CAH and contact angle, θ. However, if the magnitude of θ falls in the range of 20° to 140°, then the potential energy barrier is only a weak function of the contact angle. In other words, the potential energy barrier largely depends on CAH but not on the contact angles for $20° < \theta < 140°$.

3 Measurement of interfacial parameters

3.1 Measurement of contact angle

In this study, the contact angle and CAH were measured using a commercial contact angle goniometer. The static sessile drop method was adopted to measure the contact angle. The profile of the sessile liquid drop on a solid surface was acquired, and the contact angle was then determined. The volume of the liquid drop was fixed at 3 μL for each measurement, so that the effect of the weight of the liquid drop on the contact angle could be ignored. The contact angles of the sample surfaces with the specimen lubricants changed with time and required a few seconds to reach a stable value. Figure 3 shows the measurements of the contact angle on two different sample solid surfaces, EGC (an oleophobic coating) and a steel surface, with glycerol. The stable contact angle was selected as a reference for the hydrodynamic lubrication tests.

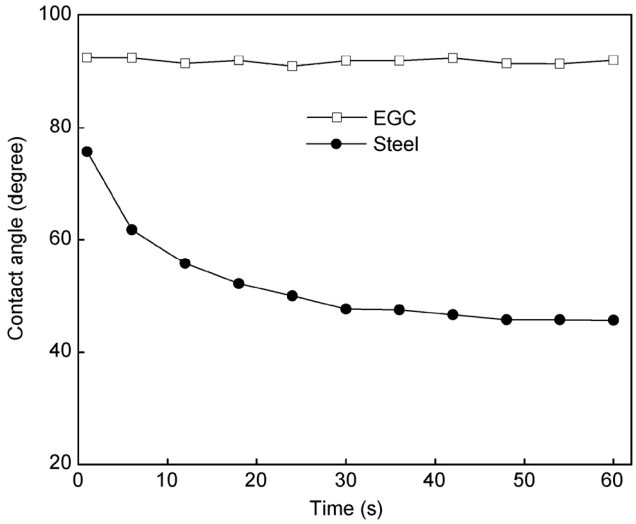

Fig. 3 Change in contact angle with time (with 99 wt% glycerol).

3.2 Measurement of CAH

CAH can be obtained using a dynamic sessile drop, the principle of which is shown in Fig. 4. The dynamic sessile drop method is similar to the static sessile drop method but requires the volume of the liquid drop to be changed. The maximum contact angle can be reached without increasing the liquid/solid interface area by adding liquid into the drop. The measured largest contact angle is the advancing contact angle. The measured minimum contact angle, found by reducing the volume of the liquid drop, is defined as the receding contact angle. The difference between the advancing and receding contact angles is the measured CAH.

3.3 Measurement of surface energy and SP

The polar and dispersive components of the solid and liquid surface tensions were identified beforehand to calculate the SP (Eq. (4)). Following the suggestion of Kalin and Polajnar [16, 17], the OWRK [21] model was applied for solid surface tension measurement. Demineralized water (polar) and hexadecane (non-polar) were selected as the model liquids. Table 1 lists the details of the surface tension of the model liquids. The contact angles of the target solid surface with the two model liquids were first measured. Based on the measured contact angle, the surface tension of the solid surface was then calculated with the OWRK model [21].

The surface tension of the sample lubricants used in this study was determined through a pendant drop.

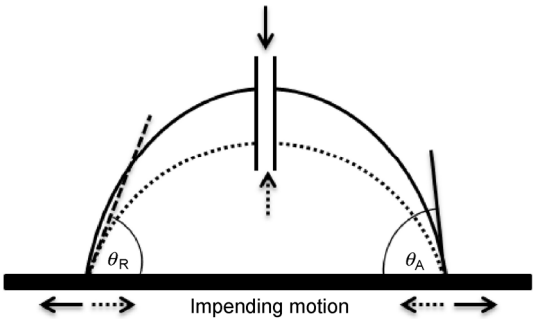

Fig. 4 Advancing and receding contact angles, θ_A and θ_R, of a sessile liquid droplet on a solid surface.

Table 1 Surface tension and its components for model liquids.

Model liquids	Total surface tension (mN/m)	Dispersive component (mN/m)	Polar component (mN/m)
Water	72.80	21.80	51.00
Hexadecane	27.60	27.60	0

A pendant drop is a drop suspended from a needle. The shape of the drop is determined by the relationship between the liquid surface tension and gravity. From the shadow image of the pendant drop, the surface tension of the liquid was calculated using the Young–Laplace equation.

4 Apparatus for the lubrication study

The lubrication behavior was examined using a fixed-incline slider test rig [25]. Figure 5 shows the schematic bearing contact of this apparatus. A rotating glass disk and a stationary slider constitute the sliding contact. The film thickness was measured with interferometry [25, 26] by the projection of a coherent light beam onto the lubricating contact via the glass disk. The top surface of the glass disk was coated with a thin chromium Cr layer (20% reflectance) for beam splitting and then with another protective SiO_2 layer (200 nm thick). The lubricant was thus bounded by the surfaces of the glass disk and the slider. The slider was lifted up when the glass disk began rotating. The film thickness was obtained with the change in interference fringe orders at an arbitrarily selected spot on the bearing contact during start-up (accelerating) and die-down (decelerating). The change in the fringe order is generally a non-integral number. The total change in film thickness was calculated from the

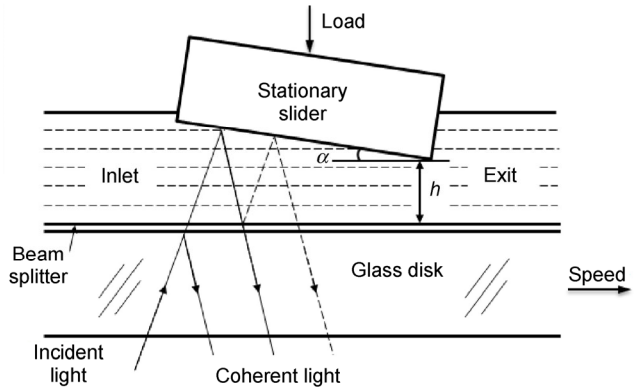

Fig. 5 Schematic illustration of the test rig.

integral and fractional parts of the change in the fringe order with a conventional interference equation and multi-beam interference based on the change in intensity [27], respectively.

5 Specimen surface and lubricant

Five sliders of identical size (4 mm (Breadth, B) × 9 mm (Length, L)) and different surface materials were adopted. Table 2 lists the properties of the slider surface materials and roughness. Three steel sliders were used, and their surface materials were steel (no coating), an EGC coating (a type of oleophobic coating, provided by the SKF research center), and an anti-fingerprint coating AFC (a commercial hydro/oleophobic thin film coating with CF_3 bonds for the protection of phone touchscreens from oils and water). Two glass sliders with different surface materials were also used. One was coated with Cr only, and the other one had an additional SiO_2 coating on top of the reflective Cr layer. In total, five surfaces were utilized in this study. Table 2 indicates that the roughness of these surfaces was of a few nanometers, with the exception of the EGC surface, which was relatively rough and reached approximately 0.05 μm.

Three lubricants were used in this study: 65 wt% glycerol, 99 wt% glycerol, and PAO40. The solute of glycerol solutions is deionized water. Table 3 shows the properties of these lubricants. The contact angle, CAH, and the SP of the sliding surfaces with these lubricants were measured. All the specimens were cleansed with the same procedure. The specimens were first rinsed with alcohol in an ultrasonic bath for 30 min. Then, cleaning tissues were applied to remove the remaining alcohol on the slider surface. Finally, the samples were blow-dried for 5 min. Each test was repeated six times, and their average values were used. The tests were carried out in a controlled environment with an ambient temperature of 22 ± 1 ℃ and a humidity of 60% ± 2%. Given that glycerol is hydroscopic, every test was completed within 20 min, and flesh glycerol was applied for each set of experiments.

Table 2 Surface roughness and materials of sliders.

Slider	Bulk material	Surface layer	Roughness (nm)
#1	Steel	Steel	6
#2	Steel	EGC	49
#3	Steel	AFC*	9
#4	Glass	Cr	2
#5	Glass	SiO_2	2

* Anti-fingerprint coating.

Table 3 Properties of lubricants used in the experiments.

Lubricant	Dynamic viscosity (22 ℃, mPas)	Refractive index
65% glycerol	14	1.45
99% glycerol	704	1.47
PAO40	880	1.47

6 Experimental results and discussion

The values of the distinct interfacial parameters of the five slider surfaces with a 65% glycerol solution were measured and tabulated, as shown in Table 4. The values are listed in ascending order of the contact angle. The EGC, which was described as a hydro/oleophobic coating by the supplier, had the largest contact angle of 105°, whereas the others had less than 90°. The SP is shown to be in reverse order, with the EGC having the lowest SP (−46.0). Figure 6 shows the contact angle measurements at the five specimen surfaces with the 65% glycerol solution. The liquid drop required marginally different levels of time to spread before obtaining the final contact angle on all the specimen surfaces, with the exception of the EGC, in which the contact angle was close to constant throughout the experiment.

The lubrication tests were conducted with a constant load of 5 N and a fixed inclination of the slider

Table 4 Interfacial parameters of slider surfaces with 65% glycerol solution.

Slider surface	Surface tension (mN/m)	Contact angle (°)	CAH (°)	θ_R (°)	$\cos\theta_R - \cos\theta_A$	SP
Steel	60.61	$37.9^{+9.2}_{-6.9}$	47.7	0	0.327	10.33
SiO_2	25.09	$51.0^{+9.0}_{-8.2}$	30.5	22.1	0.320	10.27
Cr	34.01	$65.3^{+4.6}_{-5.2}$	29.4	37.5	0.400	4.23
AFC	54.56	$87.0^{+3.3}_{-1.7}$	49.6	45.7	0.791	−17.91
EGC	47.22	$105.0^{+2.2}_{-1.1}$	16.2	92.4	0.277	−45.99
Correlation	0.580	−0.631	0.965	−0.821	0.550	0.679

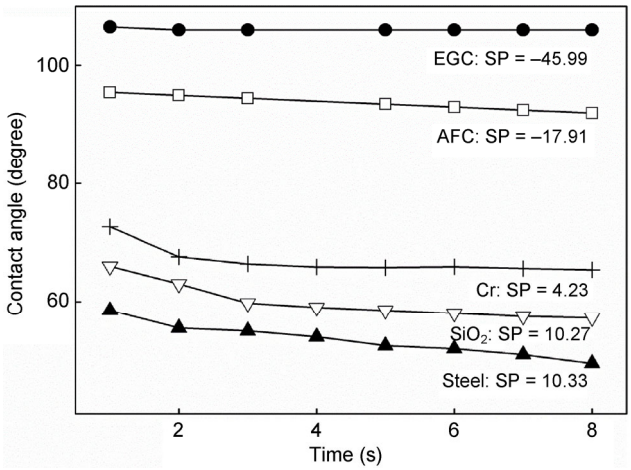

Fig. 6 Temporal change in contact angle (65 wt% glycerol).

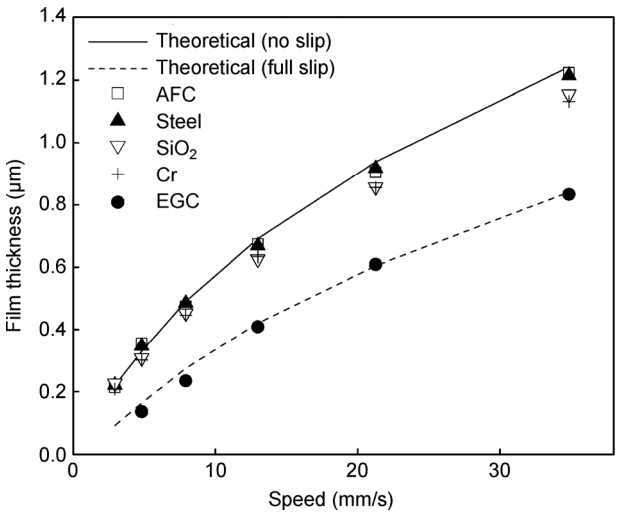

Fig. 7 Change in film thickness with speed (65 wt% glycerol, load: 5 N).

at 1:2,036. The change in film thickness of the 65% glycerol solution against the speed of the glass disk is shown in Fig. 7. Two theoretical film thickness-speed curves of no-slip and full-slip are plotted in Fig. 7, in order to depict the lubrication process. The curve with no-slip conditions was found from the solution of the classical Reynolds equation (with K = 6 in Eq. (10)). The other was obtained by solving the extended Reynolds equation with full-slip boundary conditions at the static slider surface (K = 3 in Eq. (10)) [1]. The full-slip form of Eq. (10) can be derived by considering the critical shear stress on the static slider surface to be zero:

$$\frac{\partial}{\partial x}\left(h^3\frac{\partial p}{\partial x}\right)+\frac{\partial}{\partial y}\left(h^3\frac{\partial p}{\partial y}\right)=Ku\eta\frac{\mathrm{d}h}{\mathrm{d}x} \qquad (10)$$

where K is either 6 (for no-slip) or 3 (for full-slip conditions), h is the local film thickness, p is the pressure, u is the entrainment speed, and η is the dynamic viscosity. As shown in Fig. 7, all the film thicknesses were located in the region bounded by the two theoretical curves, indicating that critical shear stress decreases (i.e., a reduction in adhesion strength) with the drop of film thickness [28, 29]. As shown in Fig. 7, the film thickness can be separated into three groups. The film thickness generated by EGC was the lowest and was significantly lower than the no-slip theoretical curve. This finding implies that the molecular bonding between EGC and 65% glycerol is relatively weak. Furthermore, the film thickness variation with speed corresponded well with the hydrodynamic lubrication theory under full-slip conditions. The film thickness that corresponded to the SiO_2 and Cr surfaces was almost the same and was significantly larger than that generated by the EGC. The film thickness generated by the steel and AFC surfaces was the largest and coincided well with the hydrodynamic lubrication theory with no-slip boundary conditions (i.e., no slip appeared at the steel and AFC surfaces in the lubrication test). All tests were conducted under the same experimental

conditions, but with different materials of the slider surfaces. Although the roughness of EGC coating was relatively large, it remained smaller than the minimum measured film thickness by an order of magnitude. Hence, the effect of roughness on the lubrication behavior could be ignored. Therefore, the difference in film thickness in this experiment can only be attributed to the surface or interfacial effect.

The correlations of film thickness at the highest speed with different interfacial parameters, including contact angle, CAH, θ_R, $\cos\theta_R - \cos\theta_A$, SP, and surface energy, are shown in Fig. 8. The film thickness decreased largely with the increase in contact angle as shown in Fig. 8(a). This observation conforms to the general concept that large contact angles correspond to weak adhesive strengths between the liquid and the solid surface, but a scattered data point of the AFC slider was observed. The contact angle of the AFC slider surface was the second largest among all the sliders, but it generated a relatively large film thickness. The correlations with surface energy and θ_R were unsatisfactory (Figs. 8(b) and 8(c)). Although the difference in surface energy and θ_R between the steel and AFC were large, the lubricating film thickness generated by these surfaces was almost the same. No apparent relationship was observed between the SP and lubricating film thickness, as shown in Fig. 8(d). The SPs of AFC and steel surfaces with 65% glycerol solution were markedly different, although they generated the same film thickness. The film thicknesses generated by SiO_2- and Cr-coated surfaces were smaller than that of steel, but their SPs were almost identical to the SP that corresponded to steel, most notably for the SiO_2 surface. Figure 8(e) shows the correlation between lubrication film thickness and the difference of $\cos\theta_R$ and $\cos\theta_A$. MacDougall and Ockrent [30] indicated that the adhesion force between the molecules of liquid and solid surfaces is proportional to $\gamma_L(\cos\theta_R - \cos\theta_A)$. Thus, the interface with a small value of $\cos\theta_R - \cos\theta_A$ had weak adhesion strength, which easily leads to slippage. However, as shown in Fig. 8(e), the difference in $\cos\theta_R - \cos\theta_A$ values between steel, SiO_2, Cr, and EGC was relatively small, most notably between steel and SiO_2, but the film thickness generated by these surfaces varied in a large range. The film thickness generated with steel and AFC was almost the same, although the $\cos\theta_R - \cos\theta_A$ value between these surfaces was large. In contrast, Fig. 8(f) shows that film thickness and CAH were strongly correlated. The correlation value between

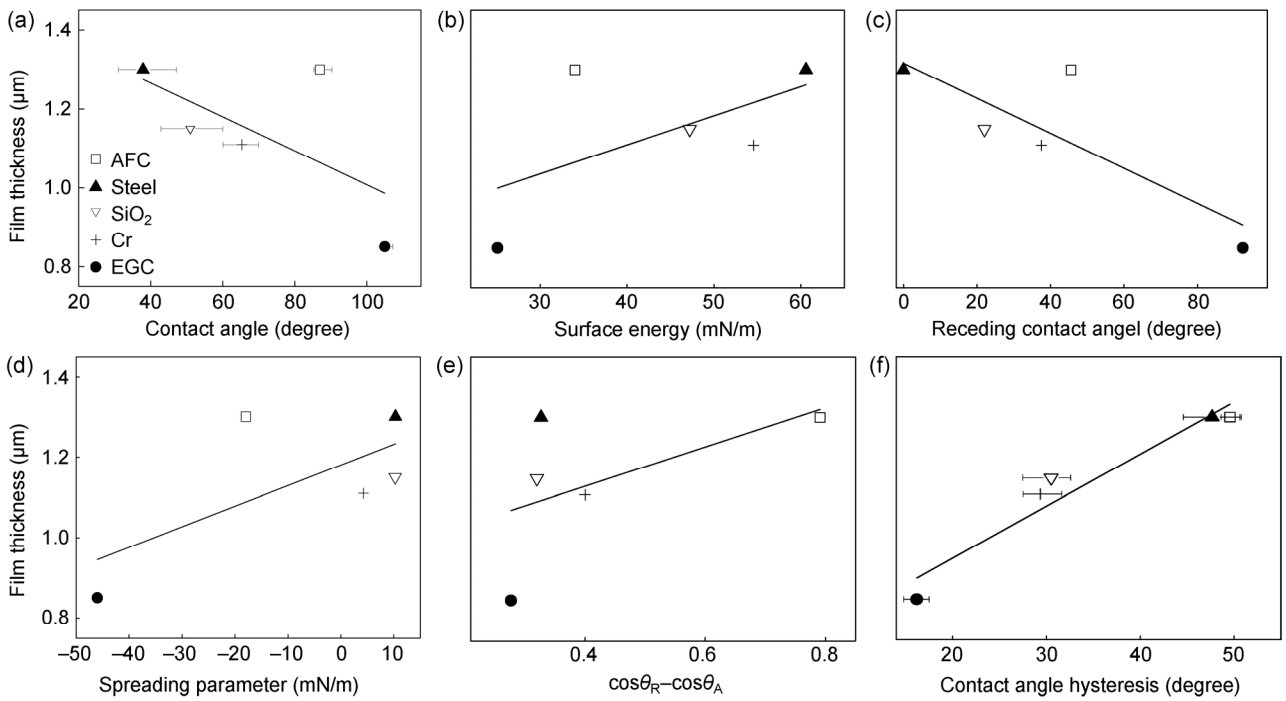

Fig. 8 Correlation of film thickness and (a) contact angle; (b) surface energy of solid surfaces; (c) θ_R; (d) SP; (e) $\cos\theta_R - \cos\theta_A$; and (f) CAH.

these interfacial parameters with lubrication film thickness is listed in Table 4. The correlation value between CAH and the film thickness was 0.965, which is significantly closer to 1 than the other parameters. This value indicates that CAH is the best interfacial parameter in determining lubrication behavior.

Hydrodynamic lubrication tests were repeated with a second glycerol solution of higher concentration (99% glycerol) for two different loads. The two with the largest difference in CAH, the steel and EGC surfaces, were tested. The measured interfacial parameters of these surfaces are tabulated in Table 5. Figure 9 shows the change in film thickness against speed. The film thickness generated by EGC was significantly smaller than that of the steel surface. Furthermore, the thickness could not be measured under low speeds due to its exceedingly small value. The low film thickness of EGC was attributed to its small CAH. Table 5 shows that the CAH of EGC with 99% glycerol is about half of the steel surface.

An oil-based lubricant (PAO40) was also used in the test. Figure 10 depicts the change in PAO40 film thickness against the sliding speed of the glass disk for three different loads. The data shown in Fig. 10 were obtained in two series of independent tests. One was conducted in a lower speed range (up to 10 mm/s). Two sliders with different surfaces, AFC and steel, were selected for this set of test with loads of 4 N and 10 N. These two surfaces provide roughly the same CAH and different other interfacial parameters as tabulated in Table 5. In the other test series, EGC was also included for comparison. As shown in Fig. 10, a higher speed range and lower load (2 N and 4 N) were adopted for the second set of tests. Figure 10 shows that the AFC and steel surfaces provided nearly identical film thicknesses under the entire speed range, which corresponded well with their similar values of CAH. The difference in their contact angle was large (nearly 40°), but the experimental results proved that such a considerable difference does not affect the lubrication behavior, thereby proving that no direct relationship exists between the contact angle and lubricating film thickness. It was noted that the contact angles of EGC and AFC with PAO40 were approximately the same, but the film thickness generated by EGC was significantly smaller compared to the AFC and steel surface. This result further confirmed that the contact angle is not the key parameter in determining lubrication behavior. Owing to its low CAH, the film-forming capability of EGC slider was the weakest, compared to that of steel and AFC surfaces.

The lubrication experiments described show the interfacial effect on thin film hydrodynamic lubrication. From the microscopic perspective, the interfacial parameters reflect the adhesive strength between the solid and liquid molecules. Slip behavior appears only when the liquid molecules have gained sufficient energy to overcome the adhesive strength, which then leads to the drop of lubrication film thickness from the no-slip theoretical value. Therefore, the experimental results proved that CAH is the appropriate parameter to reflect the adhesive strength between the molecules of solid and liquid, as derived by Whyman et al. [24]. Although the potential energy barrier is related to both the contact angle and CAH (as shown in Eq. (9)), it depends largely on CAH but not the contact angle for $120° < \theta < 140°$. As shown in Tables 4 and 5, all the contact angles measured in this study fell within this insensitive contact angle range, and that is why the correlation between the contact angle and lubrication film thickness is not apparent. Equation (9) indicates that it is relatively ease in

Table 5 Interfacial parameters of slider surfaces with 99% glycerol and PAO40.

Slider surface	Lubricant	Contact angle (°)	CAH (°)	θ_R (°)	$\cos\theta_R - \cos\theta_A$	SP
Steel	99% glycerol	$45.0^{+5.2}_{-4.2}$	$46.7^{+1.6}_{-1.1}$	0	0.314	1.60
EGC	99% glycerol	$89.2^{+1.1}_{-1.7}$	$22.8^{+1.1}_{-1.0}$	85.5	0.392	−64.7
Steel	PAO40	$28.5^{+3.5}_{-7.1}$	$33.6^{+1.5}_{-1.2}$	0	0.167	30.2
AFC	PAO40	$68.6^{+2.1}_{-1.3}$	$32.5^{+0.5}_{-0.9}$	45.0	0.491	15.2
EGC	PAO40	$73.9^{+1.5}_{-2.9}$	$23.0^{+1.1}_{-1.3}$	59.0	0.376	0.72

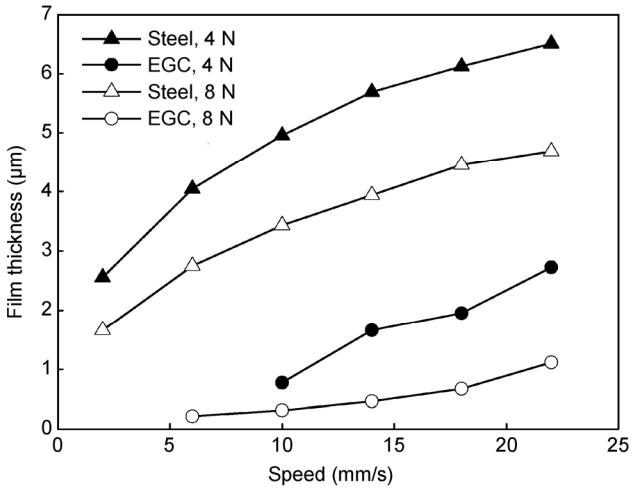

Fig. 9 Change in film thickness with speed for two different loads (99% glycerol).

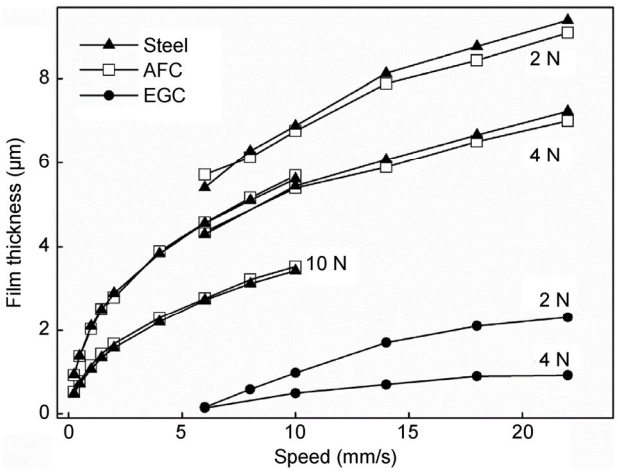

Fig. 10 Change in film thickness with speed (PAO40).

overcoming the potential energy barrier and leading to slippage for interfaces with small CAHs for the monotonous relation of CAH and the potential energy barrier. Thus, the correlation between CAH and the measured hydrodynamic lubricant film thickness is monotonous. Barrat and Bocquet [31] and Huang et al. [32] found that the boundary slip behavior becomes apparent when the contact angle exceeds 140°. This finding further verifies the experimental results described in this paper and the derivation of Whyman et al. [24].

7 Conclusion

A series of hydrodynamic lubrication experiments were performed. The experimental results demonstrated the dependency of the thin lubricating film-forming capability on the adhesive strength of the bearing surfaces. The sample surfaces included the original surface of the steel and glass (SiO_2) sliders and other surfaces prepared by coatings of various materials, including two types of oleophobic materials. The thickness of the lubricating film was measured as a function of speed and load to determine the effect of the different surfaces. The largest drop in hydrodynamic film thickness from the theoretical no-slip film thickness for a given load and speed condition was observed for an oleophobic surface (EGC), which has relatively large contact angle (up to 105° with 65% glycerol) and extremely small CAHs. In the present study, the hydrodynamic lubricating film-forming capability of the slider bearing was determined to increase with the increasing CAH of the bearing surfaces. Based on the correlation of six interfacial parameters (including contact angle, surface tension, θ_R, spreading parameter [16, 17], $(\cos\theta_R - \cos\theta_A)$, and CAH), CAH was identified as the best parameter to correlate the film-forming capability of the slider bearing. Although previous experimental studies proved that the magnitude of adhesive force (affinity between the liquid and solid molecules) also depends on the contact angle, the present findings received support from a theory derived by Whyman et al. based on a thermodynamic principle [24]. This theory stipulates that affinity is a function of both contact angle and CAH but is a weak function of contact angle for $20 < \theta < 140°$. In this study, the contact angle of all sample surfaces including steel (the most common engineering material) fell in the range of 30° to 105°. Thus, CAH was found to be the best parameter correlated with the hydrodynamic lubricating effect.

Acknowledgments

The work described in this paper was fully supported by the Research Grants Council of Hong Kong (Project No. CityU123411) and Natural Science Foundation of China (Project No. 51275252). The authors would also like to express sincere thanks to Dr. X. Zhou of SKF for providing the EGC coating in this work.

Reference

[1] Spikes H A. The half-wetted bearing: Part 1 – Extended Reynolds equation. *J Eng Tribol* **217**: 1–14 (2003)

[2] Choo J H, Glovnea R P, Forrest A K, Spikes H A. A low friction bearing based on liquid slip at the wall. *J Tribol* **129**: 611–620 (2007)

[3] Guo F, Wong P L. Full and partial boundary slippage effect on squeeze film bearings. *Tribol Int* **43**: 997–1004 (2010)

[4] Tauviqirrahman M, Ismail R, Jamari J, Schipper D J. Combined effect of texturing and boundary slippage in lubricated sliding contacts. *Tribo Int* **66**: 274–281 (2013)

[5] Craig V S J, Neo C, Williams D R M. Shear-dependent boundary slip in an aqueous Newtonian liquid. *Phys Rev Lett* **87**(5): 054504 (2001)

[6] Zhu Y X, Granick S. Rate-dependent slip of Newtonian liquid at smooth surfaces. *Phys Rev Lett* **87**(9): 096105 (2001)

[7] Spikes H A, Granick S. Equation for slip of simple liquids at smooth solid surfaces. *Langmuir* **19**: 5065–5071 (2003)

[8] Hild W, Opitz A, Schaefer J, Scherge M. The effect of wetting on the microhydrodynamics of surfaces lubricated with water and oil. *Wear* **254**: 871–875 (2003)

[9] Baudry J, Charlaix E, Tonck A, Mazuyer D. Experimental evidence for a large slip effect at a nonwetting fluid-solid interface. *Langmuir* **17**: 5232–5236 (2001)

[10] Tretheway D C, Meinhart C D. Apparent fluid slip at hydrophobic microchannel walls. *Phys Fluids* **14**: L9–L12 (2002)

[11] Guo F, Yang S, Ma C, Wong P. Experimental study on lubrication film thickness under different interface wettabilities. *Tribol Lett* **54**: 81–88 (2014)

[12] Bongaerts J, Fourtouni K, Stokes J. Soft-tribology: lubrication in a compliant PDMS–PDMS contact. *Tribol Int* **40**: 1531–1542 (2007)

[13] Joseph P, Tabeling P. Direct measurement of the apparent slip length. *Phys Rev E* **71**: 035303 (2005)

[14] Kikuchi K, Mochizuki O. Micro PIV measurement of slip flow on a hydrogel surface. *Meas Sci Technol* **25**: 065702 (2014)

[15] Ponjavic A, Chennaoui M, Wong J S S. Through-thickness velocity profile measurements in an elastohydrodynamic contact. *Tribo Lett* **50**(2): 261–277 (2013)

[16] Kalin M, Polajnar M. The correlation between the surface energy, the contact angle and the spreading parameter, and their relevance for the wetting behavior of DLC with lubricating oils. *Tribol Int* **66**: 225–233 (2013).

[17] Kalin M, Polajnar M. The wetting of steel, DLC coatings, ceramics and polymers with oils and water: The importance and correlations of surface energy, surface tension, contact angle and spreading. *App Surf Sci* **293**: 97–108 (2014)

[18] Fowkes F M. Attractive forces at interfaces. *J Ind & Eng Chem* **56**: 40–52 (1964)

[19] Wang D, Wang X, Liu X, Zhou F. Engineering a titanium surface with controllable oleophobicity and switchable oil adhesion. *J Phys Chem C* **114**: 9938–9944 (2010).

[20] Bhushan B, Her E K. Fabrication of superhydrophobic surfaces with high and low adhesion inspired from rose petal. *Langmuir*. **26**: 8207–8217 (2010)

[21] Owens D K, Wendt R. Estimation of the surface free energy of polymers. *J App Poly Sci* **13**: 1741–1747 (1969)

[22] Yaminsky V. Molecular mechanisms of hydrophobic *transitions. J Adhes Sci Technol* **14**: 187–233 (2000)

[23] Extrand C. Contact angles and their hysteresis as a measure of liquid-solid adhesion. *Langmuir* **20**: 4017–4021 (2004)

[24] Whyman G, Bormashenko E, Stein T. The rigorous derivation of Young, Cassie–Baxter and Wenzel equations and the analysis of the contact angle hysteresis phenomenon. *Chem Phys Lett* **450**: 355–359 (2008)

[25] Guo F, Wong P L, Fu Z, Ma C. Interferometry measurement of lubricating films in slider-on-disc contacts. *Tribol Lett* **39**: 71–79 (2010)

[26] Guo L, Wong P L, Guo F, Liu H C. Determination of thin hydrodynamic lubricating film thickness using dichromatic interferometry. *Appl Optics* **53**: 6066–6072 (2014)

[27] Guo F, Wong P L. A multi-beam intensity-based approach for lubricant film measurements in non-conformal contacts. *J Eng Tribol* **216**(5): 281–291 (2002)

[28] Ma G J, Wu C W, Zhou P. Multi-linearity algorithm for wall slip in two-dimensional gap flow. *Int J Numer Meth Eng* **69**: 2469–2484 (2007)

[29] Guo L, Wong PL, Guo F. Boundary yield stress and interfacial potential energy barrier in thin film hydrodynamic lubrication. *Tribol Lett* **62**: 7 (2016)

[30] MacDougall G, Ockrent C. Surface energy relations in liquid/solid systems. I. The adhesion of liquids to solids and a new method of determining the surface tension of liquids. *Proc Royal Soc Lond A Math Phys & Engg Sci* **981**: 151–173 (1942)

[31] Barrat J L, Bocquet L. Large slip effect at a nonwetting fluid-solid interface. *Phys Rev Lett* **82**: 4671 (1999)

[32] Huang D M, Sendner C, Horinek D, Netz R R, Bocquet L. Water slippage versus contact angle: A quasiuniversal relationship. *Phys Rev Lett* **101**: 22610 (2008)

Liang GUO. He received his Ph.D. degree from the Department of Mechanical and Biomedical Engineering, City University of Hong Kong in 2016. He is currently a postdoctoral fellow in the same department. His research interests include interfacial effect in hydrodynamic lubrication and contact mechanics.

Patrick WONG. He obtained his PhD degree from the University of Hong Kong in 1990, and his BSc degree from City University, London in 1983. Dr. Wong started his academic career in the City University of Hong Kong since 1990. He is currently an associate professor in the Department of Mechanical and Biomedical Engineering in the City University of Hong Kong. His research interests include rolling element bearings, interfacial phenomena, and lubrication.

Feng GUO. He got his Ph.D. degree in mechanical engineering from the City University of Hong Kong in 2003. He is now employed as a full-time professor in Qingdao University of Technology. His main work is concentrated on fundamental research and university education in tribology. His research interests include numerical computation of liquid film lubrication, optical interferometry for lubricating film measurement, interfaces in tribology and new lubrication techniques.